PROCEEDINGS OF SCIENCE

Form factor in $VP\gamma^*$ transitions and study of the $\eta \to \pi^+\pi^-\pi^0$ Dalitz plot at KLOE

Simona Giovannella*
Laboratori Nazionali di Frascati dell'INFN, Frascati, Italy
E-mail: simona.giovannella@lnf.infn.it

on behalf of the KLOE-2 Collaboration

The large data sample of light mesons available at KLOE provides the most precise measurements of the $\eta \to \pi^+\pi^-\pi^0$ decay dynamics and $\phi \to \eta e^+e^-$, $\phi \to \pi^0 e^+e^-$ transition form factors. Recent results on these decays will be discussed, together with perpectives on $\gamma\gamma$ physics for the KLOE-2 run.

*The 8th International Workshop on Chiral Dynamics, CD2015 ****
29 June 2015 - 03 July 2015
Pisa,Italy

*Speaker.

PoS(CD15)035

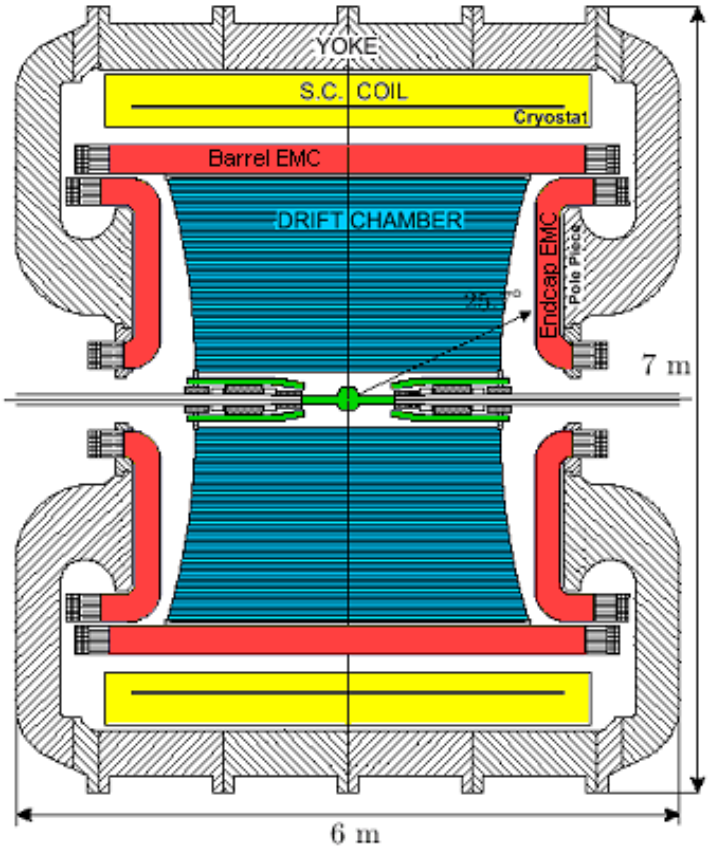

Figure 1: A transversal cross-section of the KLOE detector.

1. Introduction

The KLOE experiment [1] has collected 2.5 fb^{-1} at the e^+e^- collider DAΦNE [2], running at the peak of the ϕ resonance. An off-peak run provided also 250 pb^{-1} at 1 GeV. The detector (Fig. 1) consists of a large cylindrical drift chamber (DCH) and an electromagnetic calorimeter, surrounded by a magnetic field of 0.52 T. The beam pipe at the interaction region is spherical in shape with 10 cm radius, and it is made of a Beryllium-Aluminum alloy of 0.5 mm thickness. Low beta quadrupoles are located at about $\pm$50 cm distance from the interaction region. The drift chamber [3], 4 m in diameter and 3.3 m long, has 12,582 all-stereo tungsten sense wires and 37,746 aluminum field wires. The chamber shell is made of carbon fiber-epoxy composite with an internal wall of 1.1 mm thickness; the gas used is a 90% helium, 10% isobutane mixture. The spatial resolutions are $\sigma_{xy} \sim 150$ μm and $\sigma_z \sim 2$ mm; the momentum resolution is $\sigma(p_\perp)/p_\perp \approx 0.4\%$. Vertices are reconstructed with a spatial resolution of ~ 3 mm. The calorimeter [4] is divided into a barrel and two endcaps, for a total of 88 modules, and covers 98% of the solid angle. Signals from the modules are read out at both ends by photomultipliers, both in amplitude and time. The readout granularity is $\sim(4.4 \times 4.4)$ cm^2, for a total of 2440 cells arranged in five layers. The energy deposits are obtained from the signal amplitude while the arrival times and the particles

positions are obtained from the time differences. Cells close in time and space are grouped into energy clusters. The cluster energy E is the sum of the cell energies. The cluster time T and position are energy-weighted averages. Energy and time resolutions are $\sigma_E/E = 5.7\%/\sqrt{E\ (\mathrm{GeV})}$ and $\sigma_t = 57\ \mathrm{ps}/\sqrt{E\ (\mathrm{GeV})} \oplus 100\ \mathrm{ps}$, respectively. The trigger [5] uses information from both the calorimeter and the drift chamber. In the analyses described in the following, the events are selected by the calorimeter trigger, requiring two energy deposits with $E > 50$ MeV for the barrel and $E > 150$ MeV for the endcaps. A cosmic veto rejects events with at least two energy deposits above 30 MeV in the outermost calorimeter layer. Data are then analyzed by an event classification filter [6], which selects and streams various categories of events in different output files.

A new beam crossing scheme, allowing for a reduced beam size and increased luminosity, is now operating at DAΦNE [7]. The upgraded KLOE-2 detector is successfully rolled in inside this new interaction region and is ready to acquire collision data. Four tag stations [8] have been installed to detect electrons and positrons from the reaction $e^+e^- \to e^+e^-\gamma^*\gamma^* \to e^+e^-X$, to investigate $\gamma^*\gamma^* \to \pi^0/\pi\pi/\eta/\eta\pi$ physics at the ϕ resonance. An inner tracker [9] has been installed between the beam pipe and the inner wall of the DCH to increase the acceptance for low transverse momentum tracks and improve charged vertex reconstruction. Photon detection has been improved by means of a small crystal calorimeter in the very forward direction and of a tungsten-scintillating tile sampling device, instrumenting the low-beta quadrupoles of the accelerator [10]. A detailed description of the extended experimental physics program can be found in Ref. [11].

2. Transition form factor for $VP\gamma^*$ transitions

The vector to pseudoscalar transition form factor are not well described by the Vector Meson Dominance (VMD) model, as in the case of the process $\omega \to \pi^0\mu^+\mu^-$, measured by the NA60 collaboration [12]. New measurements of other $V \to P\gamma^*$ transitions are therefore needed to confirm this evidence. The only other existing experimental result come from the SND experiment, which has measured the M_{ee} invariant mass distribution of the $\phi \to \eta e^+e^-$ decay on the basis of 213 events [13]. The measurement of the form factor slope, $b_{\phi\eta} = (3.8 \pm 1.8)\,\mathrm{GeV}^{-2}$, differs by $1.6\,\sigma$'s from the VMD expectations ($b_{\phi\eta} = 1\,\mathrm{GeV}^{-2}$).

At KLOE, a detailed study of the $\phi \to \eta e^+e^-$ decay has been performed with 1.7 fb^{-1}, using the $\eta \to \pi^0\pi^0\pi^0$ final state [14]. Preselection cuts require: (i) two tracks of opposite sign originated from the interaction point (IP) plus six prompt photon candidates; (ii) a loose cut on the six photon invariant mass: $400 < M_{6\gamma} < 700$ MeV; (iii) a 3 σ cut on the recoil mass against the e^+e^- pair, $M_{\mathrm{recoil}}(ee)$. A residual background contamination, due to $\phi \to \eta\gamma$ events with photon conversion on beam pipe (BP) or drift chamber walls (DCW), is rejected by tracking back to BP/DCW surfaces the two e^+, e^- candidates and then reconstructing the electron-positron invariant mass and the distance between the two particles. Both quantities are small for the events coming from photon conversion. $\phi \to K\bar{K}$ and $\phi \to \pi^+\pi^-\pi^0$ events surviving analysis cuts have more than two pions in the final state. They are rejected using time-of-flight to the calorimeter. When an EMC cluster is connected to a track, the arrival time to the calorimeter is evaluated both with calorimeter (T_{cluster}) and drift chamber (T_{track}) information. Events with an e^+, e^- candidate outside a 3 σ's window on the $DT = T_{\mathrm{track}} - T_{\mathrm{cluster}}$ variable are rejected. Comparison between data and Monte Carlo events at different steps of the analysis is reported in Fig. 2. At the end of the analysis chain, 30,577 events

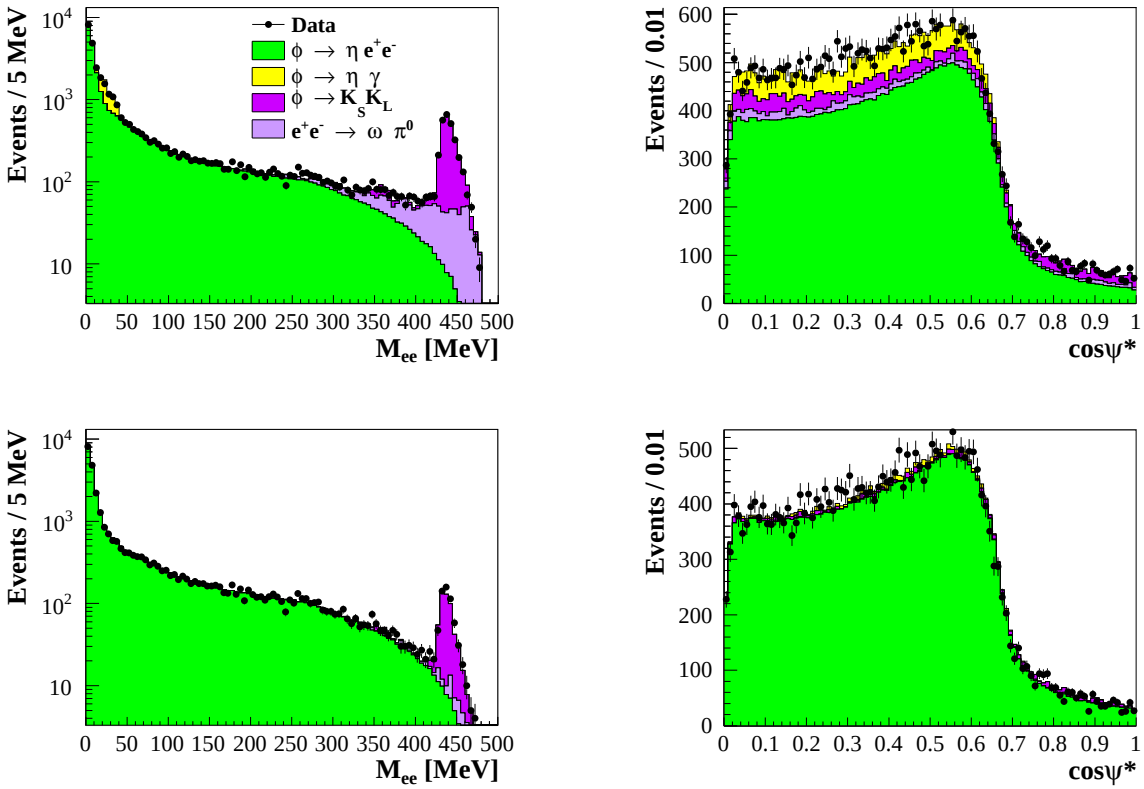

Figure 2: $\phi \to \eta e^+e^-$: data-MC comparison for the di-lepton invariant mass (left) and the $\cos\psi^*$ variable (right), after the cut on $M_{\rm recoil}(ee)$ (top) and at the end of the analysis chain (bottom).

are selected, with a residual background contamination of $\sim 3\%$. After background subraction, the measured branching fraction for the $\phi \to \eta e^+e^-$ process is:

$$BR(\phi \to \eta e^+e^-) = (1.075 \pm 0.007 \pm 0.038) \times 10^{-4}, \tag{2.1}$$

much more precise compared with the present PDG average of $(1.15 \pm 0.10) \times 10^{-4}$. The slope of the transition form factor, $b_{\phi\eta}$, has been obtained from a fit to the di-lepton invariant mass using the decay parametrization from Ref. [15]:

$$b_{\phi\eta} = (1.17 \pm 0.10^{+0.07}_{-0.11})\ \text{GeV}^{-2}, \tag{2.2}$$

in agreement with VMD predictions. Fit results are reported in Fig. 3. The modulus squared of the transition form factor, $|F_{\phi\eta}(q^2)|^2$, as a function of the e^+e^- invariant mass (Fig. 4) has been obtained by dividing the M_{ee} spectrum bin by bin with the corresponding distribution obtained for MC events generated with a constant transition form factor. The value of $b_{\phi\eta}$ extracted from the fit is in agreement with Eq. (2.2).

We have also studied the decay $\phi \to \pi^0 e^+e^-$, where no data are available on the transition form factor. Dedicated analysis cuts strongly reduce the main background component of Bhabha scattering events to $\sim 20\%$, which dominates for $M_{ee} > 300$ MeV (Fig. 5 center right). The other

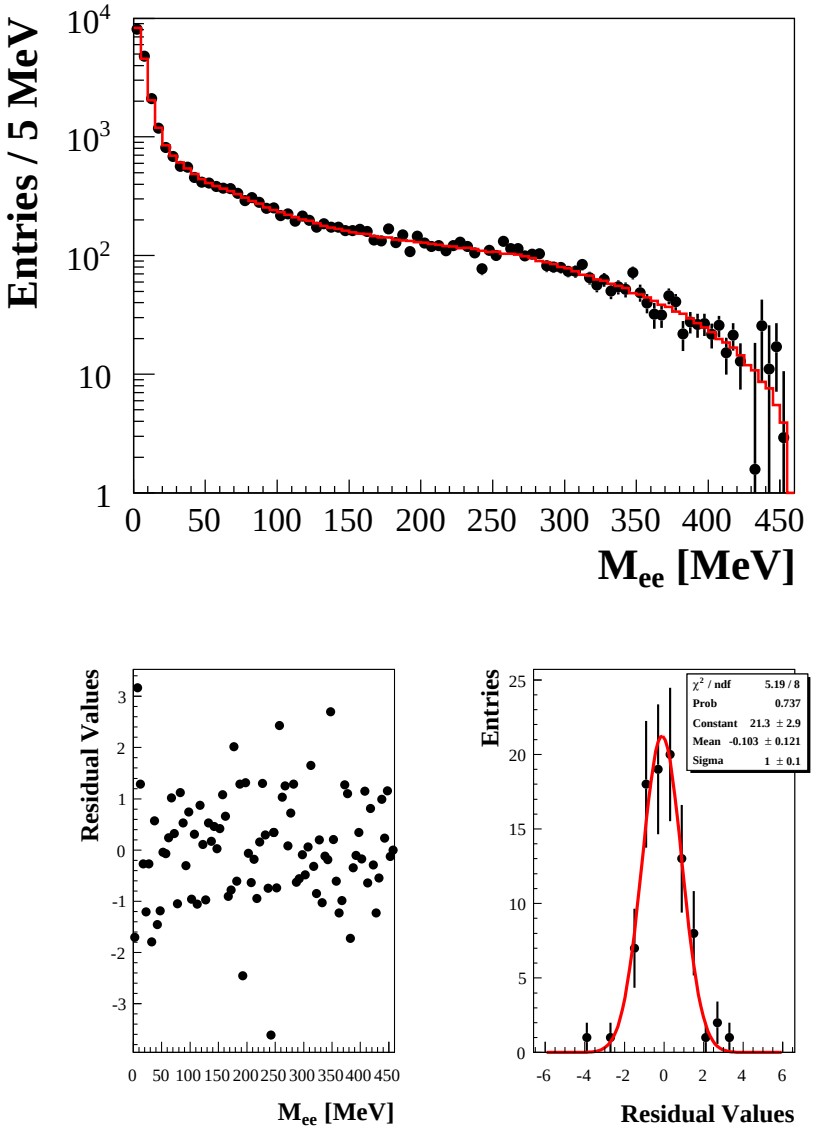

Figure 3: $\phi \to \eta e^+e^-$: fit to the di-lepton invariant mass (top), normalized fit residuals (bottom left) and Gaussian fit to the residual values (bottom right).

relevant background contribution is from ϕ radiative decays. At the end of the analysis, about 14,500 events are selected, with a total background contamination of $\sim 30\%$. Data-MC comparison is shown in Fig. 5 for different kinematical variables. The background contribution is removed bin-by-bin by subtracting the fits to each single background component from data points in the $M_{\text{recoil}}(ee)$ distribution (Fig. 6). The preliminary di-lepton invariant mass after background subtraction and efficiency correction is reported in Fig. 7, compared with the expected MC distribution for $|F_{\phi\pi}(q^2)|^2 = 1$. Only the statistical error is reported for data points.

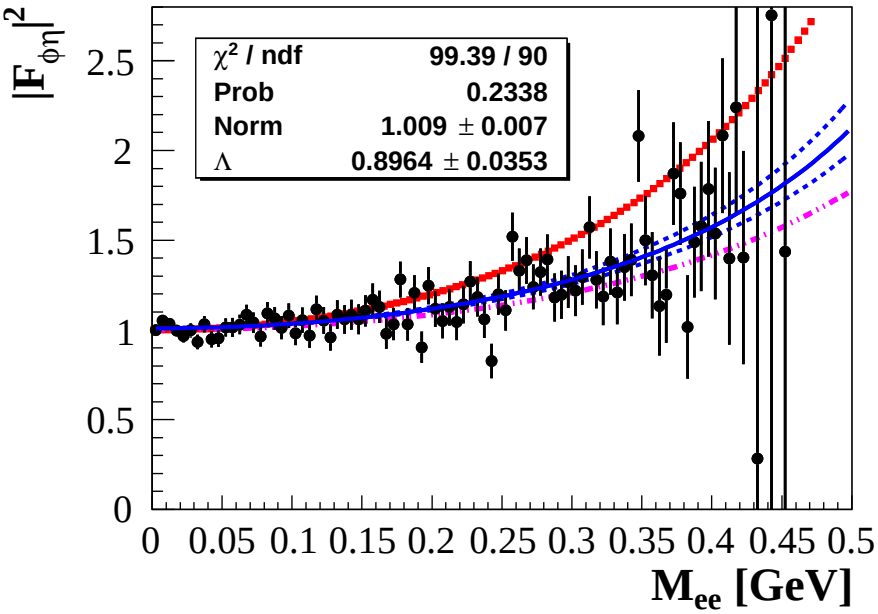

Figure 4: $\phi \to \eta e^+e^-$: $\phi\eta$ form factor as a function of the di-lepton invariant mass. The blue curve is the fit result, with its uncertainty, while in red and pink expectations from VMD and ref. [16] are reported, respectively.

3. $\eta \to \pi^+\pi^-\pi^0$ Dalitz plot

The $\eta \to \pi^+\pi^-\pi^0$ process is an isospin violating decay, sensitive to light quark mass difference [17]. Dalitz plot analysis, based on 450 pb^{-1}, has been performed at KLOE in 2008 [18] and has been used in dispersive analysis to extract the quark mass ratio [19, 20]. A new measurement has been completed, with an independent and ~ 4 times larger data set (1.7 fb^{-1}), a new analysis scheme and an improved Monte Carlo simulation.

In KLOE, light mesons are produced via radiative decays of the ϕ and are tagged by identifying the recoil monochromatic photon. The event selection requires three prompt neutral clusters in the calorimeter and two tracks with opposite curvature in the drift chamber pointing to the IP. The most energetic photon is the recoil one, and its energy is extracted using two-body decay kinematics. Decay kinematics is then exploited to assign photons to π^0. Background scaling factors are obtained by fitting data with MC distribution for two variables: the missing mass squared of the π^0 and the opening angle between photons in the π^0 rest frame (Fig. 8). Cuts on these variables are used to reduce the background contamination. The resulting efficiency for signal events is 37.6%, with a background contamination less than 1%.

The Dalitz plot density is reported in Fig. 9, where the X and Y variables are defined by means of the kinetic energies of pions: $X = \sqrt{3}(T_+ - T_-)/Q_\eta$, $Y = 3T_0/Q_\eta$. In these relations, T is the kinetic energy of the different pions in the η rest frame while $Q_\eta = m_\eta - 2m_{\pi^\pm} - m_{\pi^0}$. The Dalitz plot density has been fitted, after background subtraction, with a third order polinomial

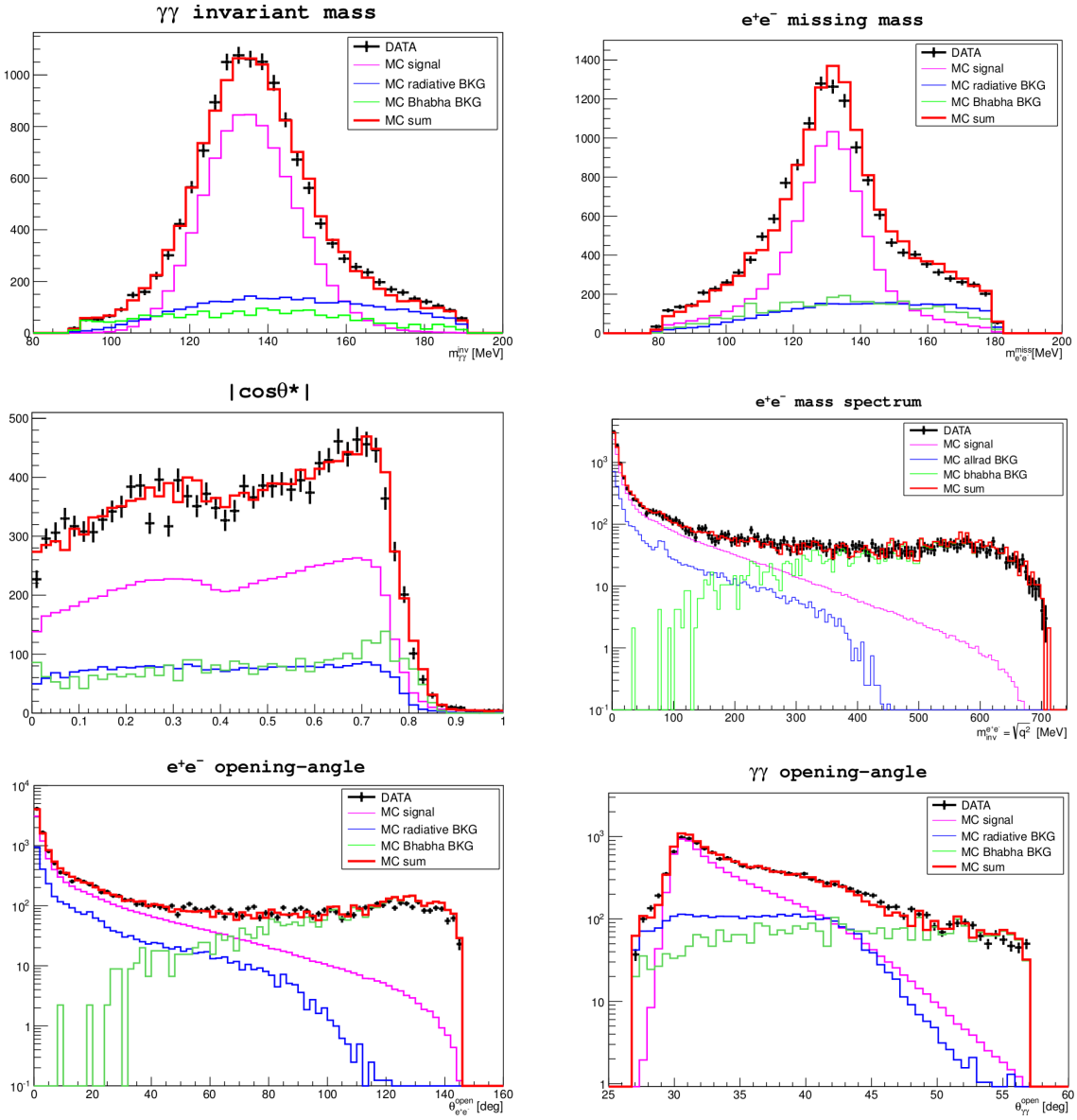

Figure 5: $\phi \to \pi^0 e^+ e^-$: data-MC comparison for the di-photon invariant mass (top left), $M_{\rm recoil}(ee)$ (top right), $\cos\psi^*$ (center left), di-lepton invariant mass (center right) and $e^+e^-/\gamma\gamma$ opening angles (bottom) at the end of the analysis chain.

expansion: $1 + aY + bY^2 + cX + dX^2 + eXY + fY^3 + gX^2Y + hXY^2 + lX^3$, folded with smearing matrix and analysis efficency. Bin size has been chosen such that it is about three times X, Y resolution. Fitting with the whole polinomial expansion, the c, e, h and l parameters are consistent with zero, as expected form C-invariance. Fixing them to zero and comparing with the previous KLOE measurement (see Tab. 1), the statistical uncertainty is reduced by about a factor of two, while improving also the systematic uncertainties. When the g parameteter is included in the fit, its value is different from zero at $3\,\sigma$ level, improving the χ^2 probability from 24% to 56%.

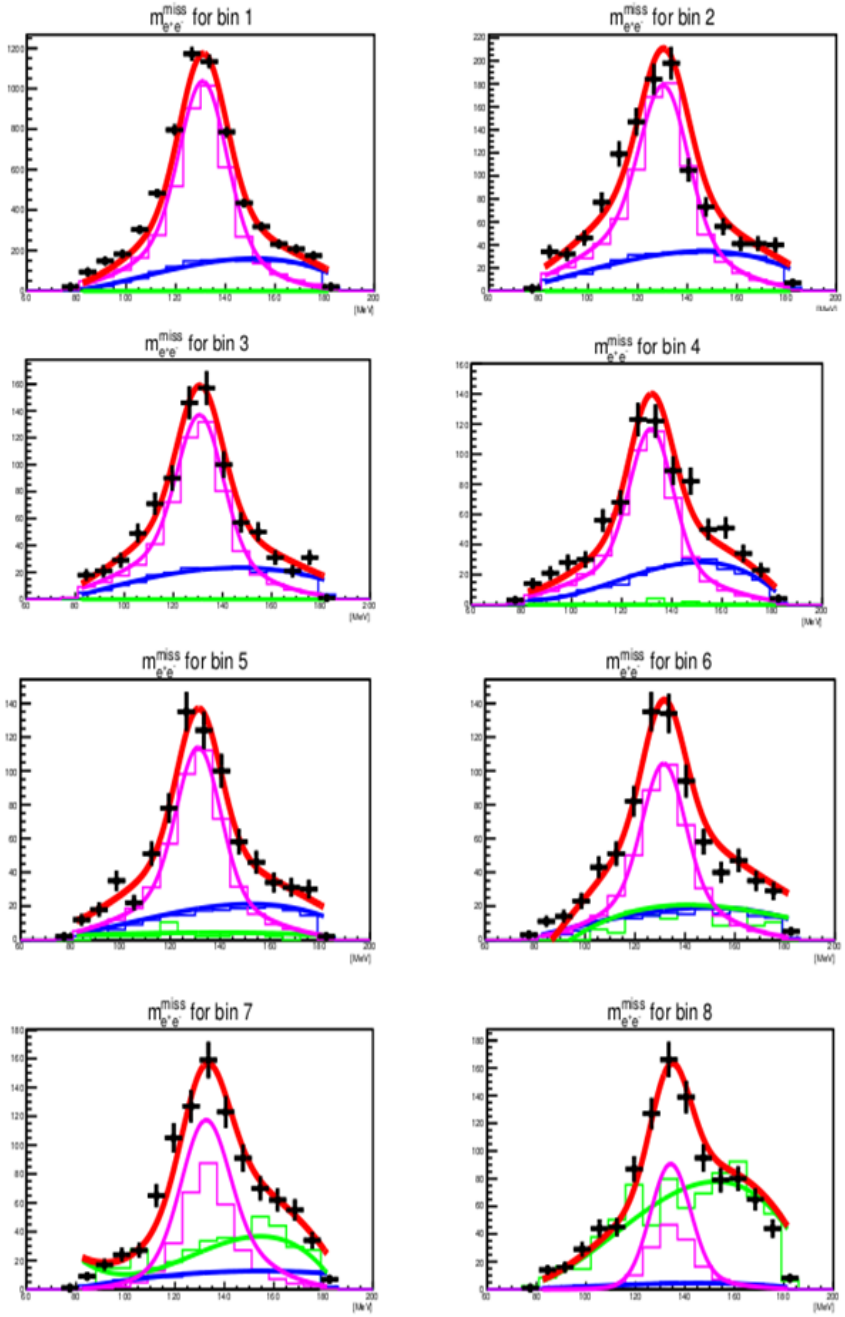

Figure 6: $\phi \to \pi^0 e^+ e^-$: fit to the $M_{\rm recoil}(ee)$ distributions for different M_{ee} values, used to extract the corresponding background components. Black dots are data, while pink, blue and green solid lines are the extracted signal, ϕ decays and Bhabha components, respectively. The red lines represent the sum of the three components.

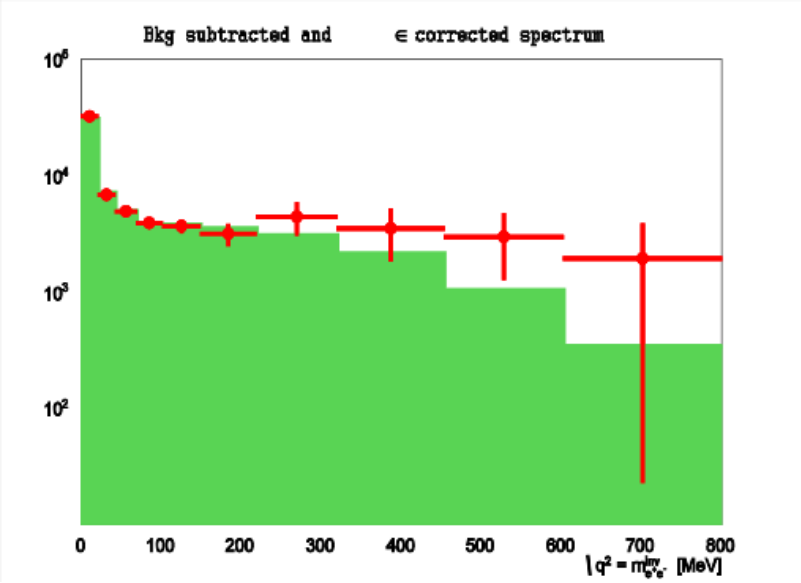

Figure 7: $\phi \to \pi^0 e^+ e^-$: preliminary background subtracted and efficiency corrected e^+e^- mass spectrum (red dots). The green histogram corresponds to the expected MC distribution for a constant transition form factor.

Table 1: Fit results for $\eta \to \pi^+\pi^-\pi^0$ Dalitz plot analysis.

	a	b	d	f	g
KLOE08	$-1.090(5)(^{+8}_{-19})$	$0.124(6)(10)$	$0.057(6)(^{+7}_{-16})$	$0.14(1)(2)$	–
KLOE15	$-1.104(3)(2)$	$0.142(3)(^{+5}_{-4})$	$0.073(3)(^{+4}_{-3})$	$0.154(6)(^{+4}_{-5})$	–
KLOE15	$-1.095(3)(^{+3}_{-2})$	$0.145(3)(5)$	$0.081(3)(^{+6}_{-5})$	$0.141(7)(^{+7}_{-8})$	$-0.044(9)(^{+12}_{-13})$

The smearing matrix of the $\eta \to \pi^+\pi^-\pi^0$ Dalitz plot is very close to diagonal. For this reason, acceptance corrected data have been used to directly fit theory. Fit results are in agreement with parameters in Tab. 1 within 1 $\sigma_{\rm fit}$.

4. $\gamma\gamma$ physics

The gamma-gamma couplings and partial widths of mesons provide information about their structure and can be measured in the $e^+e^- \to e^+e^-\gamma^*\gamma^* \to e^+e^-X$ processes, where X is a generic $J^{PC} = 0^{\pm+}, 2^{\pm+}$ final state. In the low-energy region accessible at DAΦNE, several existing measurements are affected by large uncertainties.

At KLOE, where there is no tagging of the outgoing e^+e^-, $\gamma\gamma$ interactions have been studied using off-peak data (240 pb^{-1} collected at $\sqrt{s} = 1$ GeV), to avoid backgrounds from ϕ decays. The η partial width, $\Gamma(\eta \to \gamma\gamma)$, is extracted from the measurement of the $e^+e^- \to e^+e^-\eta$ cross section, using both neutral and charged $\eta \to \pi\pi\pi$ decay channels [21]. The main background is due to the $e^+e^- \to \eta\gamma$ reaction, with an undetected recoil photon. After reducing background components with specific kinematical cuts, signal events are extracted by fitting with the expected Monte Carlo components the two-dimentional plot $M^2_{\rm miss}$–$p_{L/T}$ (Figs. 10, 11), where $M^2_{\rm miss}$ is the

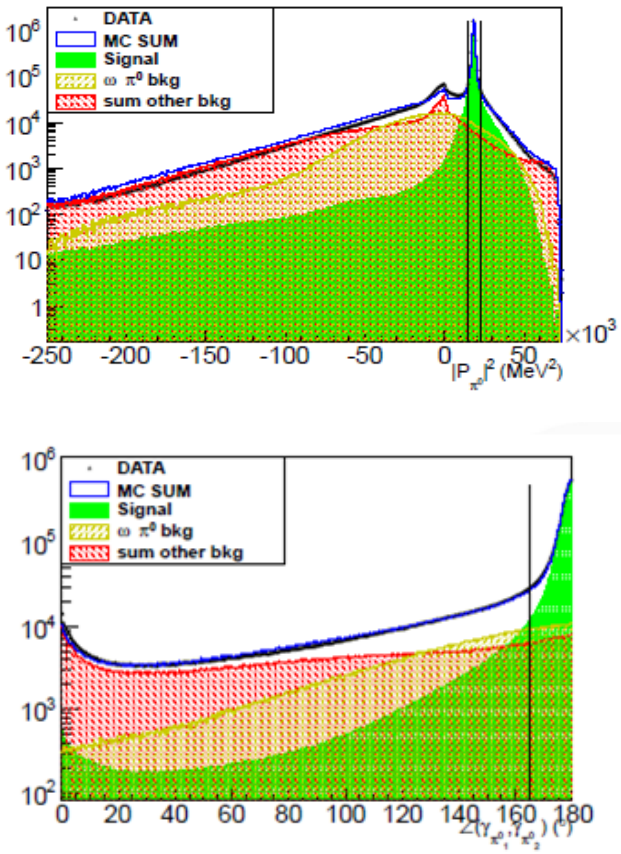

Figure 8: $\eta \to \pi^+\pi^-\pi^0$: data-MC comparison for the missing mass squared of the π^0 (top) and the opening angle between photons in the π^0 rest frame (bottom). The vertical lines represent the selection cuts.

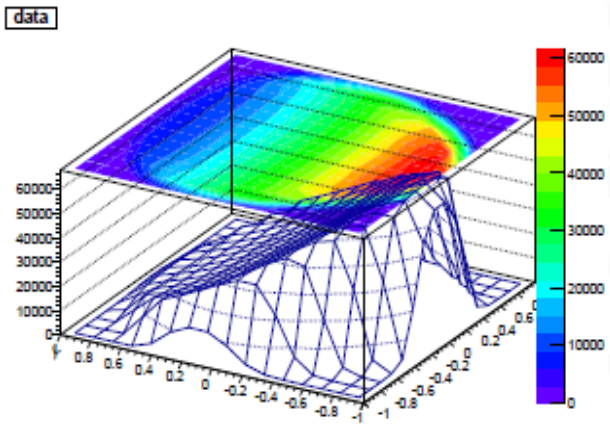

Figure 9: $\eta \to \pi^+\pi^-\pi^0$: Dalitz plot at the end of the analysis chain.

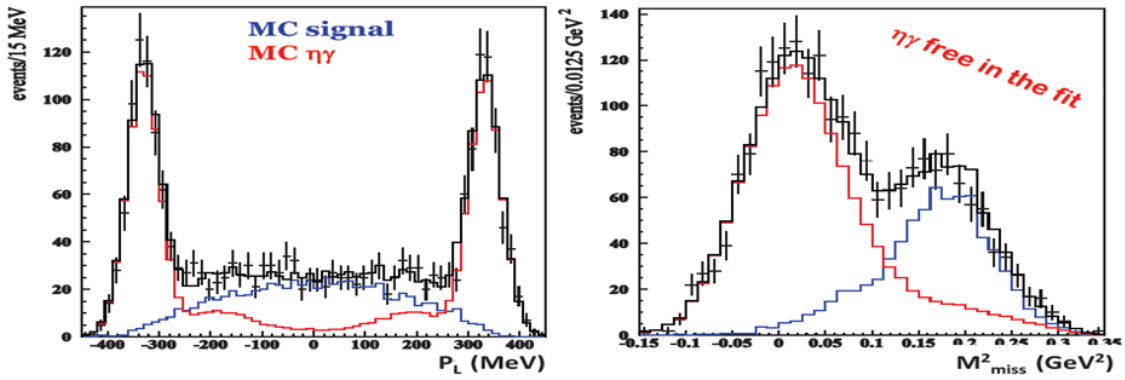

Figure 10: $\gamma\gamma \to \eta$: η longitudinal momentum (left) and M^2_{miss} distribution (right) for $\eta \to \pi^0\pi^0\pi^0$ events. Points with error bars are data, black solid histogram is fit result. The main components are signal (blue) and $\phi \to \eta\gamma$ events (red).

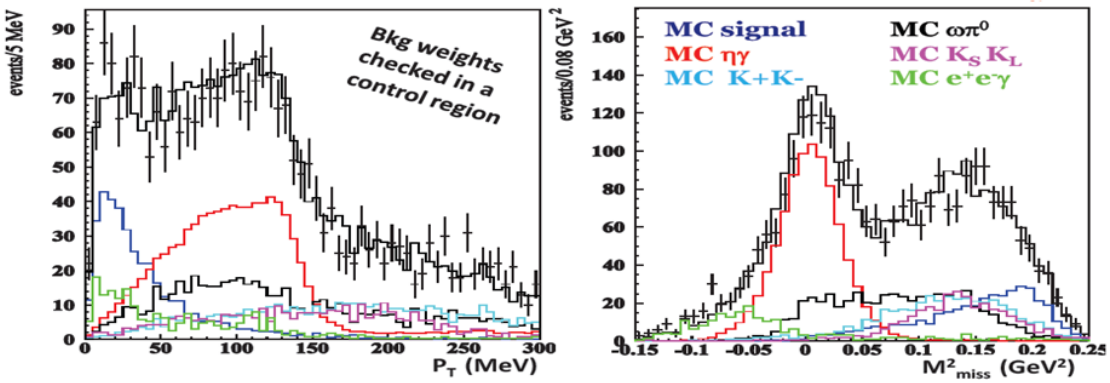

Figure 11: $\gamma\gamma \to \eta$: η tranverse momentum (left) and M^2_{miss} distribution (right) for $\eta \to \pi^+\pi^-\pi^0$ events. Points with error bars are data, black solid histogram is fit result. Different components are reported in colors.

squared missing mass and $p_{L/T}$ is the η longitudinal/transverse momentum in the $\pi^0\pi^0\pi^0/\pi^+\pi^-\pi^0$ decay. Combining the two measurements, the extracted value for the production cross section is:

$$\sigma(e^+e^- \to e^+e^-\eta) = (32.7 \pm 1.3_{\text{stat}} \pm 0.7_{\text{syst}})\ \text{pb} \tag{4.1}$$

This value is used to extract the most precise measurement of the $\eta \to \gamma\gamma$ partial width:

$$\Gamma(\eta \to \gamma\gamma) = (520 \pm 20_{\text{stat}} \pm 13_{\text{syst}})\ \text{eV}\,. \tag{4.2}$$

The upgrade of the KLOE-2 detector, with four stations installed to tag electrons and positrons from the reaction $e^+e^- \to e^+e^-\gamma^*\gamma^* \to e^+e^-X$, will give the opportunity to investigate $\gamma\gamma$ physics also at the ϕ resonance for the reactions $\gamma\gamma \to \pi^0/\pi\pi/\eta/\eta\pi$ [11]. Single pseudoscalar production will improve the determination of the two–photon decay widths of these mesons, $\Gamma_{\gamma\gamma}$. For the π^0 meson, the most precise measurement is obtained exploiting the Primakoff effect, reaching an

accuracy of 2.8% [22]. At KLOE-2, the coincidence between the KLOE central detector and the HET taggers will provide a very clean sample of ~ 1900 $\gamma\gamma \to \pi^0$ events per fb^{-1}, with background from radiative Bhabha scattering events being rejected by using the coincidence between the central detector and the HET stations. An accuracy of 1% on $\Gamma_{\gamma\gamma}(\pi^0)$ is reachable with 5-6 fb^{-1}, matching the current theory precision. With the same amount of data, the measurement of the $\pi^0 \to \gamma\gamma^*$ transition form factor in the space-like region at low momentum transfer for the virtual photon will be possible with 5-6% accuracy. The KLOE-2 measurement will cover an unexploited region of the momentum transfer. For the form factor measurement, the coincidence between the central detector and one of the HET stations will be used. The two discussed measurements are important for the theoretical evaluation of the hadronic light-by-light contribution to the muon magnetic anomaly, that is limited by the knowledge of the pseudoscalar transition form factor [23].

References

[1] KLOE Collaboration, LNF-92/019 (IR) (1992) and LNF-93/002 (IR) (1993).

[2] S. Guiducci *et al.*, Procs. of the 2001 Particle Accelerator Conference (Chicago, Illinois, USA), P. Lucas S. Webber Eds., 2001, 353.

[3] KLOE Collaboration, M. Adinolfi *et al.*, Nucl. Inst. and Meth. A 488 (2002) 51.

[4] KLOE Collaboration, M. Adinolfi *et al.*, Nucl. Inst. and Meth. A 482 (2002) 364.

[5] M. Adinolfi *et al.*, Nucl. Inst. and Meth. A 492 (2002) 134.

[6] F. Ambrosino *et al.*, Nucl. Inst. and Meth. A 534 (2004) 403.

[7] C. Milardi *et al.*, ICFA Beam Dyn. Newslett. 48 (2009) 23.

[8] D. Babusci *et al.*, Acta Phys. Polon. B 46 (2015) 81.

[9] A. Di Cicco *et al.*, Acta Phys. Polon. B 46 (2015) 73.

[10] F. Happacher *et al.*, Acta Phys. Polon. B 46 (2015) 87.

[11] G. Amelino-Camelia *et al.*, Eur. Phys. J. C 68 (2010) 619.

[12] S. Damjanovic *et al.*, Phys. Lett. B 677 (2009) 260.

[13] M. N. Achasov *et al.*, Phys. Lett. B 504 (2001) 275.

[14] KLOE-2 Collaboration, D. Babusci *et al.*, Phys. Lett. B 742 (2015) 1.

[15] L.G. Landsberg, Phys. Rep. 128 (1985) 301.

[16] C. Terschlusen and S. Leupold, Phys. Lett. B 691 (2010) 191.

[17] H. Leutwyler, Mod. Ph. Lett. A 28 (2013) 1360014.

[18] F. Ambrosino *et al.*, JHEP 05 (2008) 006.

[19] G. Colangelo *et al.*, PoS(EPS-HEP2011)304.

[20] K. Kampf *et al.*, Phys. Rev. D 84(2011) 114015.

[21] D. Babusci *et al.*, JHEP 01 (2013) 199.

[22] PrimEx Collaboration, I. Larin *et al.*, Phys. Rev. Lett. 106 (2011) 162303.

[23] D. Babusci *et al.*, Eur. Phys. J. C 72 (2012) 1917.